Available online at www.sciencedirect.com
ScienceDirect
Journal of Magnetic Resonance 188 (2007) 380–386
JMR Journal of Magnetic Resonance
www.elsevier.com/locate/jmr

Communication

Magnetic resonance force microscopy combined with surface topography

S. Tsuji [a,b,*], Y. Yoshinari [a,b], E. Kawai [a,b], K. Nakajima [a], H.S. Park [c], D. Shindo [c]

[a] *Advanced Technology Division, JEOL Ltd., 3-1-2 Musashino, Akishima, Tokyo 196-8558, Japan*
[b] *CREST, JST, 4-1-8 Honcho Kawaguchi, Saitama 332-0012, Japan*
[c] *Institute of Multidisciplinary Research for Advanced Materials, Tohoku University, Sendai 980-8577, Japan*

Received 8 February 2007; revised 20 July 2007
Available online 10 August 2007

Abstract

A new method of surface microscopy is proposed, which combines three-dimensional electron spin resonance imaging by magnetic resonance force microscopy (MRFM) and topographic imaging of the sample surface by scanning force microscopy (SFM). In order to demonstrate its potential for the identification of microscale objects, the individual and combined images are used to provide the locations, shapes and spin density distributions of target phantom objects. We report spatial resolution in MRFM of $2.8 \times 2.8 \times 2.0\mu m^3$. This could be improved to the theoretical limit of $0.08 \times 0.08 \times 0.04\mu m^3$ through reduction of the thermal noise by cooling to cryogenic temperatures ~0.5 K. We believe that this type of microscopy will become a very useful tool for the investigation of anomalies induced in surfaces by materials buried below the surface.

Keywords: MRFM; ESR; ESR imaging; AFM

1. Introduction

It is well known that in a solid electronic state and material condensation below the surface can alter the surface structure some distance away. Scanning force microscopy (SFM), which has frequently been used to observe surface topography, can detect anomalies on the surface at atomic resolution. However, SFM is unable to identify the fundamental origins of such anomalies, for instance whether they are caused by a particular compound or a defect below the surface. Magnetic resonance force microscopy (MRFM) [1,2] is one type of SFM capable of performing magnetic resonance imaging (MRI) [3–9] with remarkable sensitivity and spatial resolution. The prominent work of single spin detection [10] has demonstrated the potential of MRFM as a tool for observing individual spins, but realizing such performance for routine daily imaging measurements is still challenging. A variety of interesting physical, chemical and biological phenomena can still be observed at the micron scale, so that the establishment of this new MRFM technique is important for investigations at this resolution.

In this communication, we show experimental results performed by a new method which combines three-dimensional (3D) electron spin resonance imaging by MRFM and topographic imaging of the sample surface by SFM on a model system consisting of phantom particles. Both measurements were made using the same experimental set-up, free of hardware adjustment, so that the two images precisely coincide. This allows us to identify the location of the target materials in the monochromatic surface image as highlighted objects in the MRFM image. Furthermore, since MRFM is based on magnetic resonance and can visualize spin distribution inside the sample, this type of microscopy technique can be applied to investigate how surfaces are influenced by materials buried beneath them.

* Corresponding author. Fax: +81 42 546 7225.
E-mail address: stsuji@jeol.co.jp (S. Tsuji).
URL: http://www.jeol.com (S. Tsuji).

1090-7807/$ - see front matter © 2007 Elsevier Inc. All rights reserved.
doi:10.1016/j.jmr.2007.07.010

2. Experiments

Fig. 1 illustrates our experimental setup for MRFM and SFM measurements. The sample, shown in Fig. 1(a), consists of two kinds of material. One is a glass bead, and the other two are particles of diphenylpicrylhydrazil (DPPH) containing radicals. The two DPPH particles with sizes 5–8 μm and an 8.8 μm glass bead were glued to a commercial cantilever (MikroMasch CSC12/Tipless). The cantilever resonant frequency with the particles was $f_c \approx 14.915$ kHz with $Q \approx 8490$, and the observed noise amplitude at f_c was $\sqrt{S} \sim 0.417 \text{Å}/\sqrt{\text{Hz}}$. An estimation of the force sensitivity is not straightforward since our observations of the motion of the cantilever were made at a point approximately 60% from the cantilever open end, not precisely at the point where the samples were placed. Following Ref. [11], we estimate a correction factor $c \simeq 4.3$, giving $\sqrt{S_{\text{corr}}} \sim 0.417 \times 4.3 = 1.79$ $\text{Å}/\sqrt{\text{Hz}}$. We deduce the force sensitivity $F_{\text{noise}}/\sqrt{B}$ from the expression $(k/Q)\sqrt{S_{\text{corr}}}$, where (k/Q) is the transfer function at f_c, k is the spring constant of the cantilever and B is the bandwidth of the measurement. Using $k = 0.03$ N/m from the cantilever specification gives $F_{\text{noise}}/\sqrt{B} \sim 0.63 \times 10^{-15} \text{N}/\sqrt{\text{Hz}}$. This is in good agreement with the theoretical thermo-mechanical force noise given by $\sqrt{4kk_BT/2\pi f_c Q} \sim 0.79 \times 10^{-15} \text{N}/\sqrt{\text{Hz}}$. The force signal F is estimated by measuring the oscillation amplitude $A = (1/c)(FQ/k)$ at f_c.

The magnetic tip, fixed on a 3D closed-loop scanner, consisted of an electropolished magnetic needle made of a sintered $Nd_2Fe_{14}B$ permanent magnet [8,12]. The original dimensions of the magnetic shaft were ~30 mm long and ~0.77 mm in diameter. After electropolishing, the total length of the residual shaft became ~10 mm. The sharpened portion was nearly conical and 1.6 mm long. An inspection of its electron microscope image revealed that the very top of this magnetic needle was rounded, with a radius of curvature estimated as 3 μm. The direction of

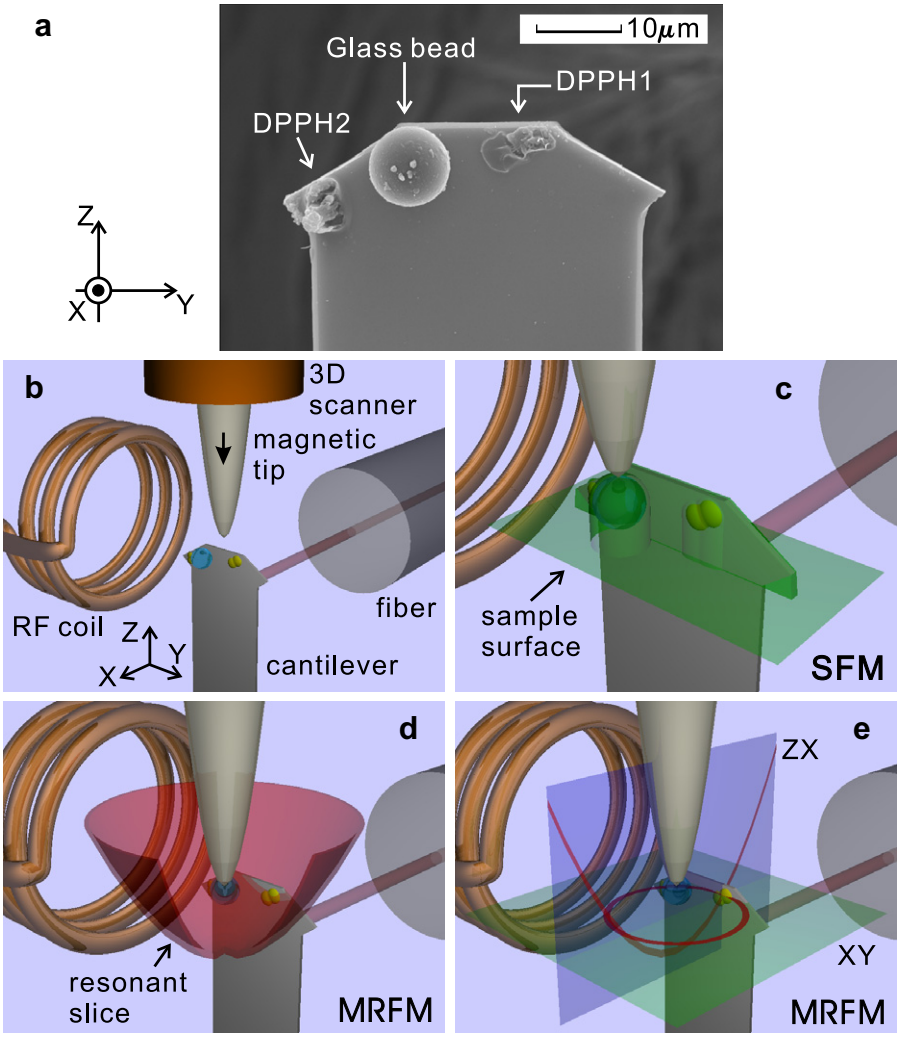

Fig. 1. (a) SEM image of our phantom sample showing two DPPH particles and a single glass bead glued on to the cantilever. (b) Schematic overview of the instrumental setup for the MRFM and SFM experiments. (c) Experimental configuration for measuring the SFM image. (d and e) Experimental configurations for measuring the MRFM image. The bowl-shaped red curve in (d) depicts a resonance slice in which spins are in resonance. The parabolic curve in the ZX-plane and the circle in the XY-plan in (e) are traces of the resonance slice cut at those planes.

magnetization was parallel to the long axis of the tip, along the Z-axis. In order to prevent the cantilever from snapping when the tip is in close proximity to the surface [10,13–15], we set the cantilever's long arm parallel to the long axis of the tip as shown in Fig. 1(b)–(e).

This magnetic tip was used as the force probe for SFM measurements to observe topographic images around the top of the sample. Fig. 1(c) is a schematic diagram of the SFM setup. With this cantilever configuration, SFM measurements were carried out using the tapping method [16]. A small piezoelectric actuator attached to the cantilever was used to excite oscillations along the X-axis. Since a huge shift of f_c due to a strong tip-sample interaction was observed as the distance between them was reduced, we were unable to keep track of f_c at the acquisition speed that would be required to obtain higher quality topographic images with the cantilever operating in the high-Q condition [17]. We therefore used a mechanical resonance around ~11 kHz originating from a cantilever holder which had a very low $Q \sim 20$. The topographic image of the sample surface was measured by recording the Z-position of the magnetic tip. First, the tip was positioned ~8 μm above the surface of the sample to set the cantilever in the absence of any tip-sample interaction and where the desired oscillation amplitude could always be obtained with a fixed voltage. Then, we turned off a phase-lock-loop which keeps the oscillation amplitude constant, so that the cantilever was excited at the fixed voltage. Then the tip was allowed to approach the sample along the Z-axis. When the monitored oscillation amplitude fell to 50% of the initial amplitude the Z-position was recorded as the sample position. This retract-approach process for measurement of the Z-position of the tip was repeated for step by step displacement of the tip position in the XY-plane.

After the sample position was identified in the SFM image, the MRFM measurement followed using the same vertical-cantilever configuration (see Fig. 1(d) and (e)). The static magnetic field necessary for the magnetic resonance was provided solely by the same magnetic tip as that used for the SFM. A parabolic resonance field was physically scanned in space by displacing the tip position. In order to observe the magnetic resonance from the unpaired electron spins in DPPH, a microwave magnetic field H_1 was applied along the Y-axis using a 0.1 mm-diameter microcoil placed in the vicinity of the sample. (This coil was present for the SFM measurements as well. Since any readjustment of the constituent parts definitely causes positional drift, we adjusted all parts at the same time.) The oscillating force exerted on the cantilever was induced using the anharmonic modulation protocol [18]. The position-dependent force signal was sampled step by step while the position of the tip was displaced in three dimensions [6].

In both SFM and MRFM, the motion of the cantilever was measured using a fiber optic interferometer [19] fitted with a laser diode having a 780 nm wave length. As we stated above, the SFM and MRFM experiments were made one after another using exactly the same experimental setup, and their images were merged together afterwards [17]. All experiments were made at room temperature under a vacuum of $\sim 10^{-3}$ Pa.

3. Results and discussion

First, Fig. 2(a) presents an example of the magnetic resonance force map in the $Y = 0$ plane taken for a single ~3 μm DPPH particle using the vertical-cantilever configu-

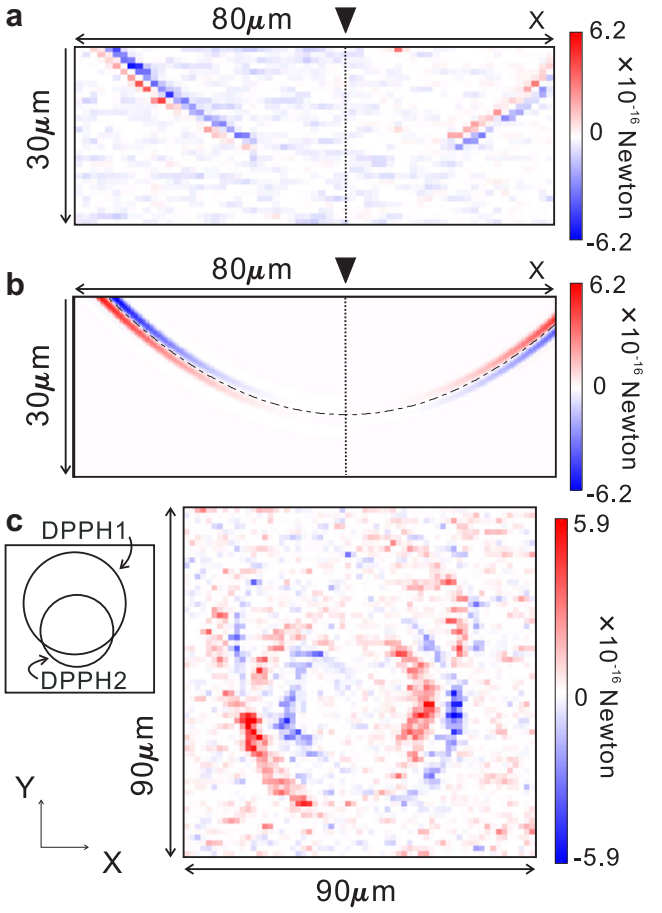

Fig. 2. (a) Example of a magnetic resonance force map in the $Y = 0$ plane taken for a single ~3 μm DPPH particle at $f_{res} = 2.5$ GHz ($H_{res} = 892.5$ G). The scan region was meshed into 64×32 pixels. The magnetic tip is shown by a small black triangle. The color grade indicates the signal intensity. The dotted line represents the anti-symmetrical plane. (b) Simulation of the force intensity. We assumed a 3 μm spherical object with spin density 2.1×10^{21} spins/cm^3. The magnetic field distribution around $H_Z = H_{res}$ was approximated by the parabolic formula [3] $H_Z = H_{res} + G_Z(Z-Z_0)+(1/2)G_{XX}(X-X_0)^2+(1/2)G_{YY}(Y-Y_0)^2$, with $G_Z = \partial H_Z/\partial Z$, $G_{XX} = \partial^2 H_Z/\partial X^2$, $G_{YY} = \partial^2 H_Z/\partial Y^2$, where (X_0, Y_0, Z_0) is the position of the apex of the paraboloid. All other parameters were experimentally known, $H_1 = 0.38$ G, AM = 100%, $H_{mod} = 13$ G, $T_1 = T_2 = 6.2 \times 10^{-8}$ s [3], $|G_Z| = 22.5$ G/μm, $|G_{XX}| = |G_{YY}| = 0.55$ G/μm^2. The broken line represents a contour of constant magnetic field $H = H_{res}$. (c) The magnetic resonance force map in the XY-plane taken for the sample shown in Fig. 1(a) at $f_{res} = 2.5$ GHz. The scan region was meshed into 64×64 pixels. The inset shows a brief sketch of our assignment of the circular contours to DPPH particles. (For interpretation of the references in colour in this figure legend, the reader is referred to the web version of this article.)

ration (as a reference, see Fig. 1(c)). The downward parabola traces a contour of magnetic resonance field $H_{res} = 892.5$ G in the vicinity of the magnetic tip. The inversion of the force intensity along the vertical scan axis Z is due to a π-phase shift arising from the derivative of the magnetic absorption peak [18]. Compared with previously reported force maps [3–8], some asymmetric character is observed along the X-axis with respect to a vertical Z (dotted) line; the tip (black triangle) at $X = 0$ may be recognized. This is supporting evidence for the true force signal in the vertical-cantilever configuration. The MRFM force is proportional to the magnetic field gradient (MFG) along the X-axis. Since the dominant MFG given by $\partial H_Z/\partial X$ changes its sign at $X = 0$, the phase of the signal must be inverted at this point. The disappearance of signals around the bottom of the contour is explained in terms of weak $\partial H_Z/\partial X$ around the symmetrical axis of the magnetic field distribution. Using experimental parameters, the calculated force map is shown in Fig. 2(b) and reproduces the observed force intensity quite well. We made similar measurements at different microwave frequencies f_{res} to characterize the field distribution in the vicinity of the tip [8], in order to estimate the remanent magnetic flux B_r of the tip. With a value for $B_r = 12.95$ kG and the known tip shape, we were able to calculate the magnetic field and MFG at any position.

Fig. 2(c) displays one of the XY-plane force maps for the sample shown in Fig. 1(a). Two circular contours were observed with paired positive and negative intensities indicating the presence of two DPPH particles; their different diameters imply that the particles sit at slightly different depths along the Z-axis. The inversion of the signal intensity along the X-axis with respect to $X = 0$ is due to the phase inversion of $\partial H_Z/\partial X$ as explained above. The 3D force map was constructed by collecting eight force maps in the XY-plane at different depth Z in a scan volume of $90 \times 90 \times 16$ μm^3; this was then divided into $64 \times 64 \times 8$ elements. The total acquisition time for completion of the mapping, including an iterative averaging eight times per element, was about six days. The stability of the stage position was better than $\sim\pm 0.17$ μm [20], and the interferometer was continuously adjusted at the most sensitive position to better than 0.5 nm. The drift of f_c was also monitored and the whole MRFM spectrometer was optimized for that value of f_c every 10 min [6]. The force map was then processed so as to restore the 3D real image using an FFT-based deconvolution algorithm with Wiener filter [3,4,21]. According to Ref. [3], the Fourier transform of the reconstructed spin density $\widehat{N}r$ is expressed by

$$\widehat{N}r = \frac{\hat{h}\widehat{F}_X}{|\hat{h}|^2 + C},$$

where $\widehat{F}_X$ and $\hat{h}$ are the Fourier transform of magnetic resonance force and point spread function(PSF), respectively. $\sqrt{C}$ is a constant determined from the maximum of $\hat{h}$ in reciprocal k-space divided by the signal-to-noise ratio of the force. In our experiment the signal-to-noise ratio was ~4.8, and we used $\sqrt{C} = 2.9 \times 10^{-28}\mathrm{N}/\sqrt{\mathrm{voxel}}$. The PSF was determined from the characterized field distribution. The restored, real 3D image is displayed in Fig. 3(a) as successive slices through the XY plane; these clearly show the presence of two objects at different depths Z.

We noticed, however, that some regions exhibit erroneous negative spin density or positive ghost images. This originates from the following subtle issues. The two bowl-shaped force surfaces observed for the two DPPH particles were mutually offset along Z. Since only one PSF can be handled in the FFT deconvolution, a mismatch in size between the observed force surfaces and the defined single PSF inevitably generates incorrect images. For instance, a PSF best matched for one force surface will be able to restore its image perfectly. But the same PSF for the other, offset force surface should possess either

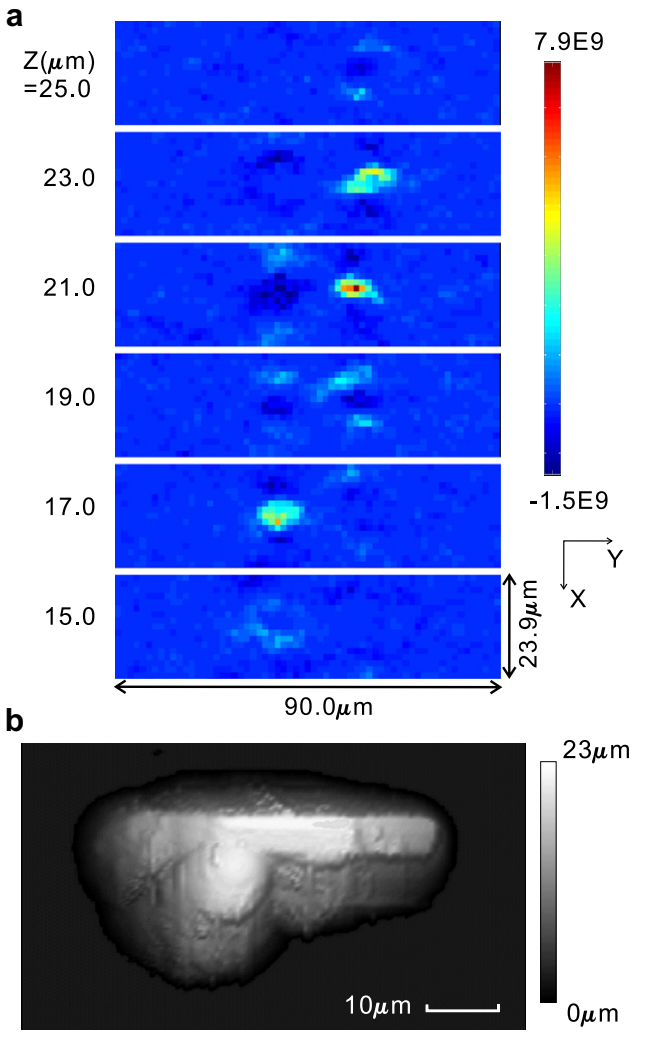

Fig. 3. (a) Restored real space images displayed in XY-planes sliced at different Z. The color grade indicates spin density per $1.41 \times 1.41 \times 2.0$ μm^3 voxel. (b) Top view of the topographical surface image. The scanned region is 40×70 μm meshed into 120×120 pixels. (For interpretation of the references in colour in this figure legend, the reader is referred to the web version of this article.)

excess or deficient structure at the brim edge of the PSF; these extraneous contributions to the deconvolution process are the origins of the ghost image. At this moment, we do not know of a better algorithm. Either have a faster computer. The images shown here were obtained when a single PSF was defined with a size intermediate between the two bowl-shaped force surfaces observed.

Fig. 3(b) shows the top-view topographic image taken with SFM. This displays a reasonable image of the sample structure. In fact, the length and trapezoidal shape of the cantilever along the Y-axis were in satisfactory agreement with the real cantilever profile provided by the manufacturer, given our experimental scan step size along the Y-axis (0.58 μm). This is evident in Fig. 4, where the side-view of the SEM image is overlaid on the MRFM image at the same scale, for comparison. In contrast, the thickness of the cantilever in the SFM image along the X-axis was found to be almost four times greater than the actual cantilever thickness of 1 μm. This exceeds the experimental error even if some broadening due to the cantilever oscillation (typically 40 nm in amplitude) is taken into account. This direction-dependent resolution problem may be explained by a presence of a fine appendix attached on the tip. The sharper tip generally provides a better SFM image. The fact that the observed line profile along the Y-axis was in good agreement is naturally interpreted in this model by noting that the stiffness of the cantilever along the cantilever width (Y) is so strong that the Y-position of the cantilever is not seriously affected by extra forces, resulting in an appropriate observation of the surface profile of the sample. On the other hand, since the cantilever's stiffness along the oscillating direction (X) is much weaker, the average X-position of the oscillating cantilever must be significantly affected by the forces. The observed thickness along the cantilever oscillation axis X is thus likely to be caused by attractive forces between the sample and the tip, which pulls the cantilever back when it is in close proximity to the sample. A convoluted broadening due to the 6 μm diameter of our magnetic tip should cause

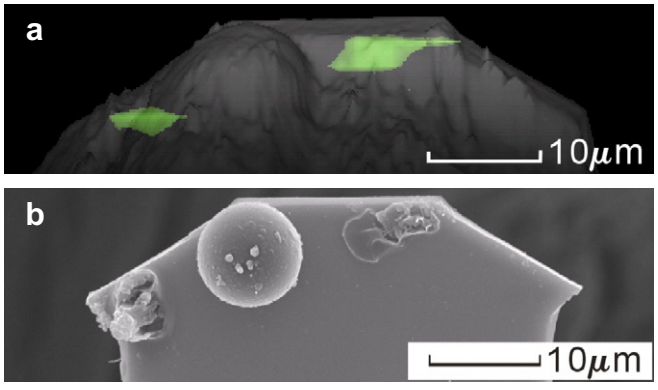

Fig. 4. Side view of the sample. (a) SFM image (grayed) is overlaid on to an MRFM image in the same area. (b) SEM image in the same scale as in (a). (For interpretation of the references in colour in this figure legend, the reader is referred to the web version of this article.)

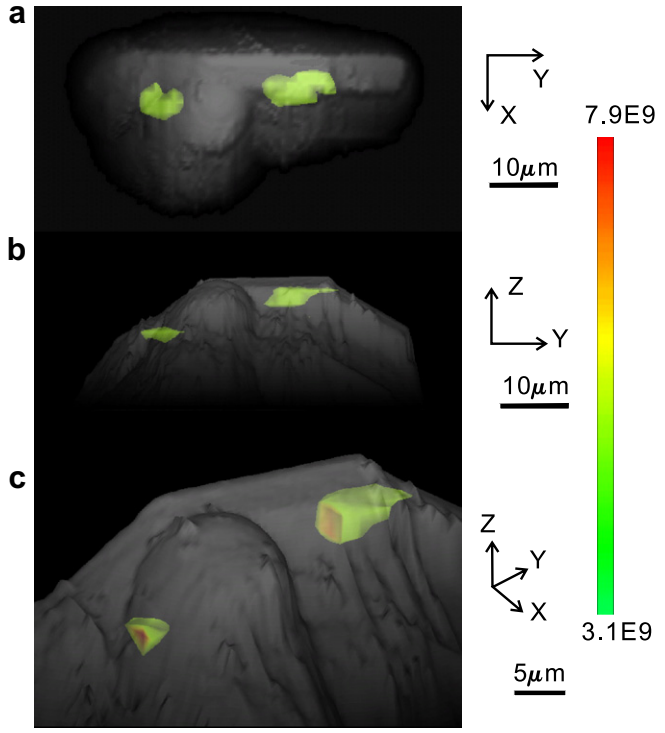

Fig. 5. Combined images of MRFM and SFM. (a) top, (b) side, and (c) magnified perspective views. Sliced cross-sections of DPPH objects are displayed in (c). (For interpretation of the references in colour in this figure legend, the reader is referred to the web version of this article.)

equivalent broadening effects for the SFM image in both the X- and Y-axes, and thus fails to explain this observation.

Finally, we present in Fig. 5 the combined 3D images of MRFM and SFM, where the display threshold for the MRFM images is set at 40% of the maximum intensity. Two distinct objects can be seen in the figures. By comparison with the SEM image of Fig. 1(a) these can be reasonably assigned to the radical-containing DPPH particles. The glass bead, which is located between the DPPH particles and clearly recognizable in the SFM image, is not present in the MRFM images because it is insensitive to magnetic resonance since free-radicals are not present. Non-negligible overlap of the restored DPPH objects on the cantilever is caused by the broadened SFM image along the X-axis as mentioned above. In particular Fig. 5(c) shows two arbitrary plane cross-sections through the DPPH images, demonstrating the usability of MRFM as an MRI spectrometer for the visualization of the internal structure of microscale objects.

4. Concluding remarks

Maintaining positional reproducibility within an instrument operating at the sub-micron scale is difficult to realize if mechanical parts are physically rearranged. This method of combining two microscopy techniques using the same experimental set-up is particularly useful for examining

relationships between the surface structure of the sample and internal spin distribution. For instance, spin-labeling techniques can also be used with MRFM to highlight the location of a designed molecule at sub-micron resolution [8].

The distribution of restored objects may not always coincide with a unit of structure such as an individual biological cell but be more localized in the unit or spread over some distance. We believe that the present microscale imaging is a potentially valuable method for the investigation of anomalies induced on the surface by spin-labeled materials buried beneath. Since nuclear magnetic resonance (NMR) with MRFM has also been reported [14,22–24], a similar visualization of the distribution of a selected nucleus by NMR might be realized.

In the present work, the spatial resolution of the reconstructed image, defined as the width over which the signal intensity decreased from 75% to 25% of its maximum on the edge of DPPH objects, was estimated to be $2.8 \times 2.8 \times 2.0\ \mu m^3$. On the other hand, the theoretical resolution, as determined by the MFG and ESR linewidths of DPPH($\sim$1 G), is calculated to be $0.08 \times 0.08 \times 0.04\ \mu m^3$. The fact that the current spatial resolution is poorer than this theoretical resolution is due both to the scan-step size of $1.4 \times 1.4 \times 2.0\ \mu m^3$ and to the limited sensitivity of a room temperature experiment. We are not equipped to observe the signal from the a voxel smaller than our practical resolution (with a reasonable signal-to-noise ratio). We have tried to estimate this sensitivity-limited resolution, equivalent to the minimum detectable voxel size as determined by the number of spins inducing the force signal (equal to the force sensitivity), divided by the spin density $\rho = 2.1 \times 10^{21}$ spins/cm^3 for DPPH. Considering that our experiments were performed with a bandwidth $B = 0.16$ Hz and with eight iterations at each position to improve the signal-to-noise ratio, the force sensitivity achievable is expected to be $F_{noise} \sim 0.11 \times 10^{-15}$ N, so the sensitivity-limited resolution is crudely estimated to be about $(0.9\ \mu m)^3$. It is expected that the theoretical resolution could be achieved by reducing the temperature to 0.5 K, where the thermal noise will be markedly reduced and the magnetization increased.

Finally, we comment on the importance of this vertical-cantilever configuration for improving the sensitivity of MRFM in the future. The expression for the force noise F_{noise} implies that this is ultimately related to the cantilever's parameters; it is essential to make k smaller, f_c and Q larger and T smaller to reduce the force noise. The use of an ultrasoft cantilever for MRFM experiments has been demonstrated where the cantilever was set normal to the sample surface to prevent it from diving into the sample [10,13–15]. From this point of view, our configuration is basically equivalent to theirs. The present work is, to our knowledge, the first to report 3D MRFM images with the cantilever oscillating parallel to a sample surface in the vertical-cantilever configuration in the presence of an external field perpendicular to the sample surface. We therefore suggest that MRFM shows promise as a nanoscale 3D imaging microscope.

Acknowledgment

We thank K. Inomata for his technical assistance of sample preparations.

References

[1] J.A. Sidles, Noninductive detection of single-proton magnetic resonance, Appl. Phys. Lett. 58 (24) (1991) 2854–2856.
[2] D. Rugar, C.S. Yannoni, J.A. Sidles, Mechanical detection of magnetic resonance, Nature (London) 360 (1992) 563–566.
[3] O. Zügar, D. Rugar, Magnetic resonance detection and imaging using force microscopy techniques, J. Appl. Phys. 75 (1994) 6211–6216.
[4] O. Zügar, S.T. Hoen, C.S. Yannoni, D. Rugar, Three-dimensional imaging with a nuclear magnetic resonance force microscope, J. Appl. Phys. 79 (1996) 1881–1884.
[5] K. Wago, D. Botkin, C.S. Yannoni, D. Rugar, Paramagnetic and ferromagnetic resonance imaging with a tip-on-cantilever magnetic resonance force microscope, Appl. Phys. Lett. 72 (1998) 2757–2759.
[6] S. Tsuji, T. Masumizu, Y. Yoshinari, Magnetic resonance imaging of isolated single liposome by magnetic resonance force microscopy, J. Magn. Reson. 167 (2004) 211–220.
[7] S. Chao, W.M. Dougherty, J.L. Garbini, J.A. Sidles, Nanometer-scale magnetic resonance imaging, Rev. Sci. Instrum. 75 (2004) 1124–1127.
[8] S. Tsuji, Y. Yoshinari, H.S. Park, D. Shindo, Three dimensional magnetic resonance imaging by magnetic resonance force microscopy with a sharp magnetic needle, J. Magn. Reson. 178 (2006) 325–328.
[9] T. Mewes, J. Kim, D.V. Pelekhov, G.N. Kakazei, P.E. Wigen, S. Batra, P.C. Hammel, Ferromagnetic resonance force microscopy studies of arrays of micron size permalloy dots, Phys. Rev. B. 74 (2006), 144424–1–6.
[10] D. Rugar, R. Budakian, H.J. Mamin, B.W. Chui, Single spin detection by magnetic resonance force microscopy, Nature 430 (2004) 329–332.
[11] K. Wago, O. Zügar, R. Kendrick, C.S. Yannoni, D. Rugar, Low-temperature magnetic resonance force detection, J. Vac. Sci. Technol. B 14 (1996) 1197–1201.
[12] H.S. Park, Y.G. Park, Y. Gao, D. Shindo, M. Inoue, Direct observation of magnetization reversal in thin $Nd_2Fe_{14}B$ film, J. Appl. Phys. 97 (2005), 033908–1–4.
[13] T.D. Stowe, T.W. Kenny, D.J. Thomson, D. Rugar, Silicon dopant imaging by dissipation force microscopy, Appl. Phys. Lett. 75 (1999) 2785–2787.
[14] S.R. Garner, S. Kuehn, J.M. Dawlaty, N.E. Jenkins, J.A. Marohn, Force-gradient detected nuclear magnetic resonance, Appl. Phys. Lett. 84 (2004) 5091.
[15] S. Kuehn, R.F. Loring, J. Marohn, Dielectric fluctuation and the origins of noncontact friction, Phys. Rev. Lett. 96 (2006), 156103–1–4.
[16] Q. Zhong, D. Inniss, K. Kjoller, V. Elings, Fractured polymer/silica. fiber surface studied by tapping mode atomic force microscopy, Surf. Sci. Lett. 290 (1993) 1688–1692.
[17] We have also tried to perform a *simultaneous* data acquisition of SFM and MRFM signals. The experimental protocol is based on a sequential phase sensitive comparison method similar to that used in Kelvin force microscopy [25]. The amplitude-regulated cantilever oscillation was excited at f_c, and we also set the MRFM experimental parameters so as to induce the MRFM signal at $f_{mod} \ll f_c$ by use of anharmonic modulation [18]. Under such conditions, when the MRFM signal appears, the force gradient acting on the cantilever has two components; one (DC) component is a static force gradient conventionally used for obtaining the topographical SFM image,

whilst the other alternating component (AC), responsible for the MRFM signal, originates from a time-dependent force gradient induced because the sample magnetization is modulated at f_{mod}. The sequential phase detection of the excited cantilever oscillation was used to obtain the respective signals. The SFM image was obtained in the first phase detection at f_c, and its demodulated signal was further evaluated in the second phase detection at f_{mod} to extract the MRFM signal. Although we have succeeded in observing 1D SFM and MRFM spectra *simultaneously*, the MRFM signal measured as a shift of the cantilever frequency was too small ~ 1 μHz even for 7 μm DPPH to carry out the imaging experiment at room temperature.

[18] K.J. Bruland, J. Krzystek, J.L. Garbini, J.A. Sidles, Anharmonic modulation for noise reduction in magnetic resonance force microscopy, Rev. Sci. Instrum. 66 (1995) 2853–2856.

[19] D. Rugar, H.J. Mamin, P. Guethner, Improved fiber-optic interferometer for atomic force microscopy, Appl. Phys. Lett. 55 (1989) 2588–2590.

[20] Three capacitance sensors are utilized for controlling the stage position in 3D. The stage stability is dependent on the distance between the sensor fixed in space and the displacing stage. We estimated the precision of position stability by measuring the standard deviation of a histogram made by a series of position data sampled every 150 ms. This was found to be ~0.17 μm when the distance was the largest by of 100 μm.

[21] W.H. Press, B.P. Flannery, S.A. Teukolsky, W.T. Vetterling, Numerical Recipes: The Art of Scientific Computing, First ed., Cambridge University Press, Cambridge, 1989.

[22] K.R. Thurber, L.E. Harrell, D.D. Smith, 170 nm nuclear magnetic resonance imaging using magnetic resonance force microscopy, J. Magn. Reson. 162 (2003) 336–340.

[23] D. Rugar, O. Zügar, S. Hoen, C.S. Yannoni, H.-M. Vieth, R.D. Kendrick, Force detection of nuclear magnetic resonance, Science 264 (1994) 1560–1563.

[24] Q. Lin, C.L. Degen, M. Tomaselli, A. Hunkeler, U. Meier, B.H. Meier, Magnetic double resonance in force microscopy, Phys. Rev. Lett. 96 (2006), 137604–1–4.

[25] M. Nonnenmacher, M. O'Boyle, H. Wickramasinghe, Kelvin probe force microscopy, Appl. Phys. Lett. 58 (1991) 2921–2923.